

Article

Separation and Extraction of Mixed Grinding Chips of Artificial Joints with Different Densities by Multiple Centrifugal Separations

Cunao Feng [†], Yujie Zhao [†], Tao Zhang, Kai Chen ^{*}, Xiaowei Li  and Dekun Zhang ^{*}

School of Materials Science and Physics, China University of Mining and Technology, Xuzhou 221116, China

^{*} Correspondence: cumtck@cumt.edu.cn (K.C.); dkzhang@cumt.edu.cn (D.Z.); Tel.: +86-13952207958 (K.C.); +86-13952207958 (D.Z.)[†] These authors contributed equally to this work.

Abstract: Aseptic loosening caused by the wear and tear of the artificial joint prosthesis after implantation is one of the main causes of artificial joint failure. Therefore, it is important to investigate the wear debris generated due to wear when developing new artificial joint materials. Aseptic loosening is related to the size, number, and morphology of wear debris, and this study proposed the separation and extraction of mixed wear debris with different density ratios of artificial joints by centrifugation to study the characteristics of different artificial joint wear and wear debris extraction rates. The results showed that multiple centrifugations to separate the mixed wear debris were able to reintroduce the wear debris on the wall of the centrifuge tube into the solution and that the wear debris extraction rate was increased. Suspensions with different density ratios of artificially jointed mixed wear debris were effectively separated by this method. The total extraction rate of the three repeated extractions compared to the first extraction rate, the extraction rate of CoCrMo wear debris increased by 6.7%, ultra-high molecular weight polyethylene (UHMWPE) wear debris increased by 15.1–23.44%, ZrO₂ wear debris increased by 10.91%, and that of polyether ether ketone (PEEK) wear debris increased by 9.95%. This method for separating and extracting wear debris from artificial joints can realize the separation of mixed wear debris from artificial joints and obtain a high extraction rate and high-quality wear debris images, investigate the wear mechanism of artificial joint implants, and provide valuable information on the wear performance of new artificial joint implants under investigation.

Keywords: different density ratios; multiple centrifugal separations; wear chips

Citation: Feng, C.; Zhao, Y.; Zhang, T.; Chen, K.; Li, X.; Zhang, D. Separation and Extraction of Mixed Grinding Chips of Artificial Joints with Different Densities by Multiple Centrifugal Separations. *Lubricants* **2022**, *10*, 226. <https://doi.org/10.3390/lubricants10090226>

Received: 14 August 2022

Accepted: 15 September 2022

Published: 19 September 2022

Publisher's Note: MDPI stays neutral with regard to jurisdictional claims in published maps and institutional affiliations.



Copyright: © 2022 by the authors. Licensee MDPI, Basel, Switzerland. This article is an open access article distributed under the terms and conditions of the Creative Commons Attribution (CC BY) license (<https://creativecommons.org/licenses/by/4.0/>).

1. Introduction

The artificial joint is implanted in the human body in a complex operating environment, such as the knee joint, where it is submerged in body fluids but also subjected to the effects of the body's impact and weight. As a result, frictional wear of the joint material after implantation is bound to produce wear debris. Aseptic loosening of the artificial joint caused by wear debris is the main mode of artificial joint failure, with a failure rate of about 10% [1–5]. Abrasive debris of different morphology [6–8], size [9–12], and composition [13,14] reflect different frictional wear mechanisms, and behaviors of artificial joints and can lead to different degrees of biological responses [15–18]. New artificial joint materials must be investigated for wear debris before they are introduced into the clinic and market [19]. Therefore, the effective separation and extraction of artificial joint wear debris from the lubricating fluid and the characterization and analysis of artificial joint wear debris are one of the key topics in the study of artificial joint materials.

Evaluation of the frictional wear performance of artificial joints is mainly performed in vitro using artificial joint simulators, in which calf serum is usually used as a simulated lubricating fluid [20]. Artificial joint wear produces a mixture of wear debris of different

shapes, sizes, and compositions [6,21,22]. The morphological characteristics of the wear debris reflect the complexity of wear, such as UHMWPE granular wear debris, are mainly formed by adhesive wear [23]. Wear debris is often considered to be the typical product of adhesive wear [23]. There are many studies exploring the relationship between UHMWPE wear debris and aseptic loosening [24–26]. Extraction and research of mixed wear debris is rarely available. Extraction and characterization of mixed wear debris play an important role in studying the tribological behavior of artificial joints, wear mechanisms, and prolonging their service life, and excellent methods for extracting abrasive chips from the lubricant of artificial joints in vitro wear tests need to be urgently explored.

Artificial joint wear debris scattered in the calf serum lubricating fluid and the surface through the electrostatic effect, hydrophobic effect, hydrophilic effect, and lubricating serum in the protein combination by the multi-layer protein are wrapped to form a protein halo. This poses a great challenge in terms of wear debris count, particle size analysis, and morphological characterization for artificial joint wear tests. Extraction of wear debris includes degradation of proteins and separation of wear debris [23]. Artificial joint wear debris extraction first needs to exclude the interference of proteins or lipids in serum, and degradation of proteins in calf serum is one of the main steps of artificial joint wear debris extraction. Another important step in the extraction of artificial wear debris is the separation and filtration of the mixed wear debris. Artificial joint wear debris is lost with the removed solution during extraction or adheres to the walls of containers, such as centrifuge tubes, which can result in poor extraction rates of artificial joint wear debris. CoCrMo, UHMWPE, and ceramics are the mainstay of research on the extraction of wear debris from artificial joint materials. Only one artificial joint wear debris was extracted, and there is little research on the separation and extraction of new artificial joints such as PEEK and hybrid abrasive chips.

Previous studies on the extraction rate of artificial joint wear debris are only for CoCrMo and ceramics [13,27,28], which are denser and easier to separate and extract from the solution. The extraction rate is low, and there is a lack of studies on the extraction rate of artificial joint wear debris such as PEEK, which are similar to the solution density. Using the traditional artificial joint wear debris extraction method [29], we proposed an extraction method of multiple centrifugal separations for mixed wear debris from artificial joints with different density ratios. This method could separate and extract the mixed wear debris effectively while improving the extraction rate of artificial joint wear debris. The results of the study provide a basis for research on the mechanism of wear debris generation and the wear mechanism of artificial joints.

2. Materials and Methods

2.1. Materials

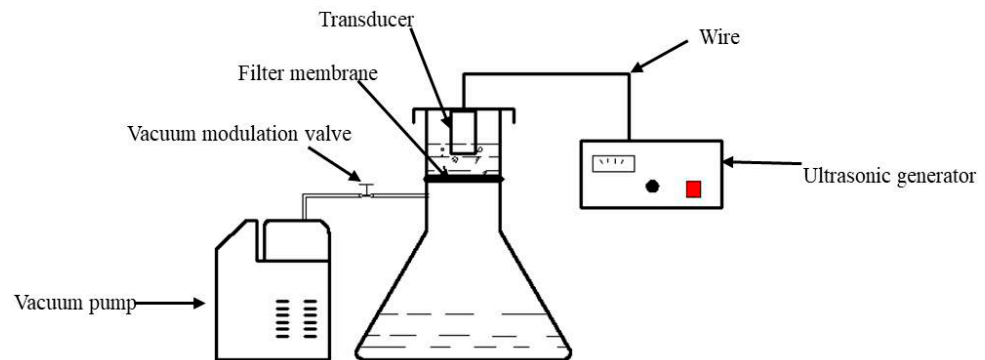
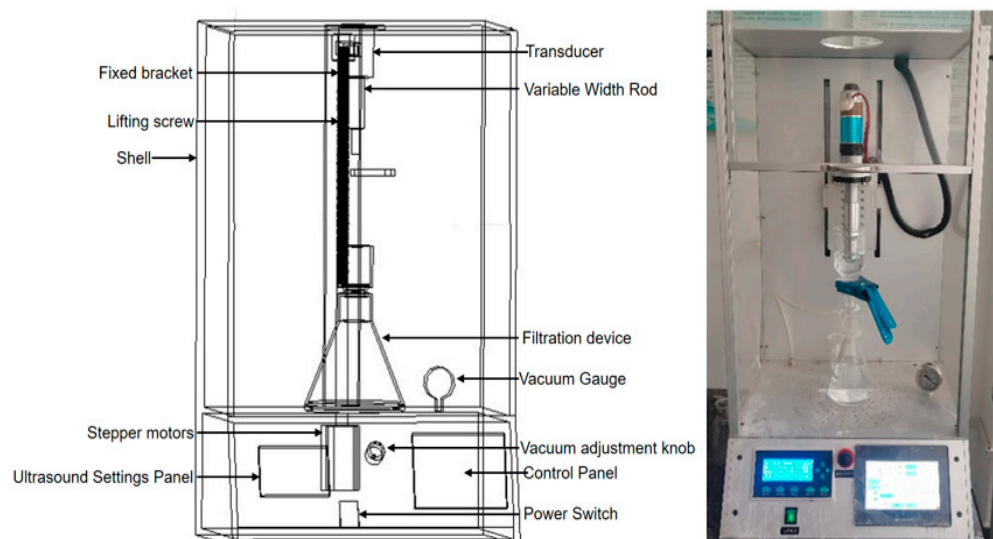
UHMWPE powder (molecular weight 600 million, Mitsui Chemicals (Shanghai)), PEEK powder (1000 mesh, medical grade, Victrex High Performance Materials Trading (Shanghai) Co., Ltd., Shanghai, China), ZrO₂ powder (50 nm, Andi Metal Materials Co., Ltd., Qinghe County, Xingtai, China), and CoCrMo powder were selected as the particles collected for wear experiments. Calf serum (protein concentration 36 mg/mL, Zhejiang Tianhang Biotechnology Company, Hangzhou, China), papain (Aladdin Biochemical Technology Co., Shanghai, China), proteinase K, sodium phosphate (Xilong Science Co., Shantou, China), ethylenediaminetetraacetic acid (EDTA) (Wuxi Yashang Chemical Co., Ltd., Wuxi, China), hydrochloric acid, trihydroxymethylaminomethane (Tris), and mixed grinding chips with different density ratios of artificial joints were also important materials in this study. Different density ratios of the artificial joint mixed grinding chips were prepared according to the artificial joint material, as shown in Table 1.

Table 1. Mixed wear debris with different density of artificial joint.

Artificial Joint Materials	Density (g/cm ³)
CoCrMo/UHMWPE	8.375/0.960
PEEK/UHMWPE	1.375/0.960
ZrO ₂ /UHMWPE	6.000/0.960

2.2. Experimental Equipment

Combining the theoretical study of ultrasound-assisted artificial joint wear debris extraction and separation and the problems in the grinding chip extraction process, this study independently developed the VN-2 type microparticle and nanoparticle separation and extraction device. The working principle diagrams of the micro-nanoparticle separation and extraction device are shown in Figure 1. Separation and extraction of microscopic and nanoparticles using the VN-2 device is a special bench-type device and consists mainly of an ultrasonic system, a vacuum filtration system, and support components. The schematic diagram and physical photos of the micro-nanoparticle separation and extraction device are shown in Figure 2.

**Figure 1.** Principle picture of separation system of VN-2 micro-nano particle isolation device.**Figure 2.** Schematic diagram and photograph of VN-2 micro-nano-particle isolation device.

2.3. Calculation of the Settling of Abrasive Chips in a Solution

2.3.1. Settling Velocity of Abrasive Chips in a Stationary Solution

The migration and diffusion of wear debris in degraded calf serum solution is essentially a matter of force and migration of particles in liquid–solid two-phase flow. The forces on the particles in the flow field are complex. If the concentration of particles in the

solution is high, the particles are agglomerated by electrostatic forces, van der Waals forces, etc., and fragmentation and reorganization occur during migration and diffusion. If the particle concentration is low, we ignore the interaction of the forces between the particles, consider the particles as individual particles to consider their forces, ignore the effect of shape on particle migration, and simplify the individual particles to the problem of settling of single spherical particles in solution. The force analysis of particles in the flow field with Newton's second law shows that [29]

$$m_p \frac{du_p}{dt} = \sum F_p + m_p g \quad (1)$$

where m_p is the particle mass (kg); u_p is the particle velocity (m/s); t is the time (s); F_p is the combined force of buoyancy, pressure gradient force, traction force, Basset force, Magnus force, Saffman force, etc. on the particle (N); and $m_p g$ is the particle gravity (N). We derive the equation of motion of the particle based on the force on the particle in the vertical direction [30].

$$m_p \frac{du_p}{dt} = -\frac{1}{8} C_D \pi d_p^2 \rho_f u_p^2 - \frac{1}{12} \pi d_p^3 \rho_f \frac{du_p}{dt} + \frac{1}{6} \pi d_p^3 g (\rho_f - \rho_p) \quad (2)$$

ρ_f is the fluid density (kg/m³), ρ_p is the particle density (kg/m³), and d_p is the diameter of the particle (m). In general, Magnus lift force and Saffman lift force is small in value and can be ignored, and Basset force only works in a very short period of particle motion; therefore, the force is ignored for particle motion analysis in the vertical direction, and C_D is the resistance coefficient.

$$m_p = \frac{4}{3} \pi \left(\frac{1}{2} \cdot d_p \right)^3 \rho_p \quad (3)$$

Substituting (3) into (2), we obtain

$$\frac{du_p}{dt} = -\frac{3\rho_f}{4\rho_p d_p} C_d u_p^2 - \frac{\rho_f}{2\rho_p} \frac{du_p}{dt} + g \left(1 - \frac{\rho_f}{\rho_p} \right) \quad (4)$$

The C_d value is related to the fluid Reynolds number [31,32]:

$$\begin{cases} C_D = \frac{24}{Re} & Re < 1 \\ C_D = \frac{24}{Re} (1 + 0.15 Re^{0.667}) & 1 \leq Re < 1000 \\ C_D = 0.44 & Re \geq 1000 \end{cases} \quad (5)$$

The fluid Reynolds number is used to characterize the flow of fluid dimensionless number.

$$Re = \frac{(\rho_p - \rho_f) g d_p^2}{18 \mu_f} \quad (6)$$

μ_f is the dynamic viscosity coefficient of the fluid (kg/(m·s)). The above Stokes resistance formula is limited in practical use, but the use of Stokes formula [33] for semi-quantitative analysis is still of some significance in theoretical analysis.

We solve the 2–4 differential equation for u_p as follows:

$$u_p = \frac{(\rho_p - \rho_f) g d_p^2}{18 \mu_f} \left(1 - e^{-\frac{18 \mu_f}{\rho_f d_p^2}} \right) \quad (7)$$

To simplify the calculation, the wear debris were regarded as spherical particles with an initial velocity of 0 m/s and a diameter d_p of 1×10^{-7} m. The density of 25% calf serum solution after protease degradation was tested to be 999.312 kg/m³, μ_f was taken as 1.004×10^{-3} Pa·s, and the settling velocity of individual spherical grinding chips of different density artificial joints in suspension was calculated by Matlab as shown in Table 2.

Table 2. Settling velocity of single spherical wear debris of different density in suspension.

Abrasive Dust	Sedimentation Velocity $\times 10^{-5}$ (mm/h)
UHMWPE	0.077
PEEK	0.723
ZrO ₂	975.960
CoCrMo	1434.960

2.3.2. Settling Velocity of a Single Wear Debris in a Centrifugal Field

In viscous liquids, particles are subject to frictional resistance and inertial resistance. Frictional resistance is caused by the zero velocity of the liquid near the surface of the object. Inertial resistance depends on the following conditions: if the pressure increases along the surface around the object, the boundary layer will be abruptly changed to the form of a vortex. Thus, the pressure on the front surface of the object to be greater than the pressure on the back surface. The equation for the head-on resistance of an object moving in a liquid is as follows.

$$F = C_x v^2 d_p^2 \rho_f \quad (8)$$

F (N), v (m/s), d (m), ρ_f (kg/m³), and C_x are the head-on resistance, particle motion speed, particle diameter, liquid density, and head-on resistance coefficient, respectively.

The head-on drag coefficient is a function of the ratio of inertia force to friction force, i.e., a function of Reynolds number, calculated as (9).

$$C_x = f(R_e) = (1.45)\alpha + 7.5/R_e \quad (9)$$

α is the angle of inclination of the pipe wall.

The Reynolds number is used to express the velocity of particle movement in a liquid medium.

$$v = \frac{R_e \mu_f}{\rho_f d_p} \quad (10)$$

Substituting (9) and (10) into (8), we obtain

$$F = \frac{C_x R_e^2 \mu^2}{\rho_f} \quad (11)$$

When the particles are moving in suspension, if the force acting on the object is constant (gravity), the object will reach a constant speed in a very short time due to the large resistance of the liquid itself and the increase in resistance with the increase in the speed of the object. In most cases, the acceleration phase of the motion can be neglected, and the final velocity of the particle motion can be determined when the liquid resistance is equal to the force acting on the particle [34,35].

If the particles in motion in the liquid in the gravitational field quickly reach a practically constant speed, the velocity of the object in the centrifugal field will increase continuously because the centrifugal inertia forces acting on the object will increase proportionally to the distance from the axis of rotation to the center of the object. Assuming that the settling particles that have reached a certain distance r from the axis of rotation continue to be subjected to constant centrifugal inertia forces when settling further, the settling velocity of the particles may also soon become constant. In the meantime, the resistance of the liquid may also increase to equal the gravitational force. As the particles gradually move away from the rotary axis, the resistance of the liquid is often less than the centrifugal inertia of the particles. The differential equation for the relative motion of the particles in the centrifugally separated liquid is as follows [36].

$$m \frac{dv}{dt} = \frac{\pi d^3}{6} \Delta \omega^2 r - \frac{C_x R_e \mu^2}{\rho_f} \quad (12)$$

m (kg), Δ (kg/m³), r (m), and ω (1/s) are the mass of the particle, the density difference between the particle and the liquid, the distance from the axis of rotation to the center of the particle, and the angular velocity of rotation, respectively.

$C_x Re$ is a factorless parameter; by deriving the value of Re and the data associated with C_x and Re , the general formula for calculating the settling velocity of solid particles in the centrifugal field is as follows.

Particle settling velocity in the laminar flow region:

$$v = \frac{d^2(\rho_p - \rho_f)j^2}{18\mu} \quad (13)$$

Particle settling velocity in the transition area:

$$v = 0.1355 \cdot \frac{d^{1.2}(\rho_p - \rho_f)^{0.733}j^{0.7333}}{\rho_f^{0.26}\mu_f^{0.46}} \quad (14)$$

Particle settling velocity in the turbulent region:

$$v = 1.75\sqrt{\frac{d_p(\rho_p - \rho_f)j}{\rho_f}} \quad (15)$$

The densities of UHMWPE, PEEK, ZrO₂, and CoCrMo are 960 kg/m³, 1375 kg/m³, 6000 kg/m³, and 8375 kg/m³, respectively. To simplify the calculation, the wear debris were considered spherical particles with a diameter d_p of 5×10^{-8} m, and r is taken as the distance of 0.06 m from the center of the selection of the particles at the center of the middle layer of the centrifugal tube. The density of the solution after degradation is 999.312 kg/m³, μ_f is taken as 1.004×10^{-3} Pa·s, the rotation speed is 10,000 r/min, and the calculation results of the wear debris settling speed are shown in Table 3.

Table 3. Settling velocity of particles in fluid with different motion states.

Abrasive Chips	Laminar Flow Area (mm/h)	Transition Area (mm/h)	Turbulent Region (mm/h)
UHMWPE	5.14	1.11	111,306.65
PEEK	48.45	5.78	311,085.42
ZrO ₂	654.78	38.90	1,142,589.63
CoCrMo	962.48	51.66	1,385,285.83

2.4. Multiple Centrifugal Separation and Extraction of Mixed Wear Debris with Different High-Density Ratios

The proteins were degraded by protease degradation method, and the extraction was achieved by multiple centrifugal separation and extraction method for different density ratios of artificial joint mixed wear debris, and the extraction process was as follows.

- (1) Sufficiently dried CoCrMo, UHMWPE, PEEK, and ZrO₂ powders were taken in amounts of 10 mg each and their mass recorded as m before the extraction of wear debris; they were mixed thoroughly according to the combination of CoCrMo/UHMWPE, PEEK/UHMWPE, and ZrO₂/UHMWPE and incubated with 10 mL of 25% calf serum solution at room temperature for 24 h.
- (2) Protein was degraded using 25 g/L sodium dodecyl sulfate, 1 g/L papain solution, and proteinase K solution diluted to 20 mg/mL with Tris-HCl solution (pH 7.6). During degradation, the pH was adjusted with sodium phosphate solution (40.99 g/L), EDTA solution (7.306 g/L), Tris (6.057 g/L), and hydrochloric acid solution. The resulting final solution was dispensed in 50 mL centrifuge tubes. The detailed degradation process was shown in Figure 3.

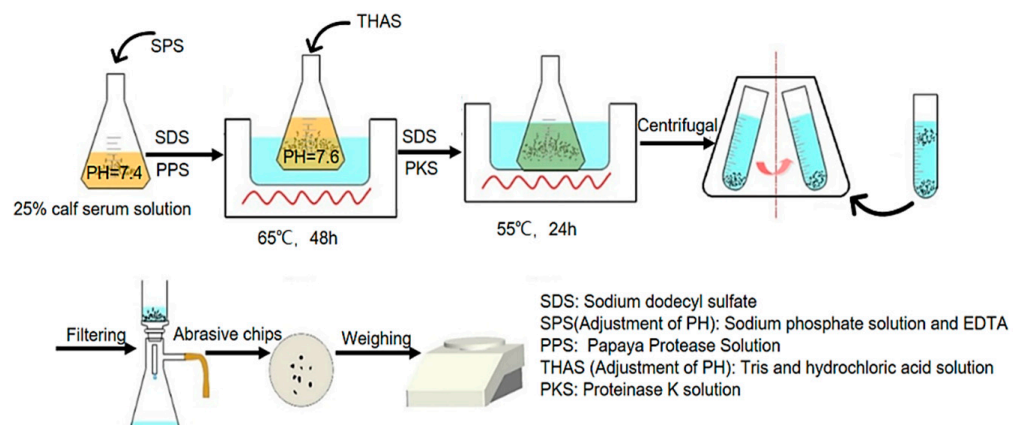


Figure 3. Flow diagram of wear debris separation by multi-centrifugation.

- (3) Centrifugation was performed at 10,000 r/min for 2 h using a high-speed centrifuge (MG15, Shanghai Maigao Scientific Instruments Co., Ltd., Shanghai, China).
- (4) The solution in the centrifuge tubes after centrifugation was divided into an upper zone (solution containing a small density of wear debris), a mixed zone (incompletely separated mixed solution), and a lower zone (solution containing a large density of wear debris) in that order. The upper and lower zone solutions were filtered, and the mixed zone solution was moved into a new centrifuge tube. After theoretical calculations and experiments, it was proven that the three zones were divided differently for different density ratios of artificial joint mixed wear debris, and the division results are shown in Table 4 and Figure 4a.

Table 4. Solution separation zone after the first three centrifugations.

Mixed Wear Debris	Upper Area (100%)	Lower Area (100%)
CoCrMo/UHMWPE	35–50	3.75–5
PEEK/UHMWPE	25–35	5–7.5
ZrO ₂ /UHMWPE	5–12	5–10

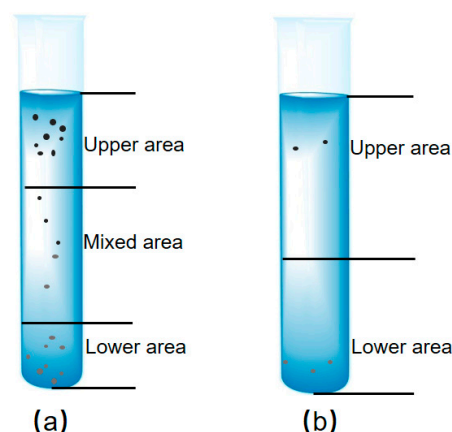


Figure 4. (a) Schematic diagram of solution isolation area after the first three centrifugations; (b) schematic diagram of solution extraction area after four or more centrifugations.

- (5) The extracted solution of the upper zone and the solution of the lower zone were filtered through a nylon filter membrane with a pore size of 0.05 μm , and the mass of the dried filter paper with wear debris was recorded as m_1 . The filter paper containing the wear debris was placed in a beaker with an appropriate amount of ethanol and shaken in an ultrasonic cleaner for 20 min. The weight of the dried filter paper with wear debris was recorded as m_2 . The mass of the extracted wear debris

was $m_1 - m_2$. The ethanol suspension containing the wear debris was dried until the ethanol evaporated completely, and the composition of the remaining wear debris was analyzed.

- (6) We rinsed the wall of the original centrifuge tube with deionized water, transferred the rinsed liquid into a new centrifuge tube of mixed zone solution, and diluted the mixed zone solution with deionized water to 2/3 of the centrifuge tube.
- (7) Then, we repeated steps 3–6 for secondary and tertiary centrifugal separation and extraction. After three centrifugal separations and extractions, the operation of step 6 and 3 was repeated in turn for the fourth centrifugal separation and extraction. The solution in the centrifuge tubes after centrifugation was divided into two zones: the upper zone (solution containing small-density wear debris) and the lower zone (solution containing large-density wear debris) in turn. It was proven that the two zones were divided differently for different density ratios of artificial joint wear debris, and the results of the division are shown in Table 5 and Figure 4b. The extraction rate results after four centrifugations were calculated until it was not possible to measure the amount of extracted particles by weighing.

Table 5. Solution separation zone after the first three centrifugations.

Mixed Wear Debris	Upper Area (100%)	Lower Area (100%)
CoCrMo/UHMWPE	70–80	20–30
PEEK/UHMWPE	45–55	45–55
ZrO ₂ /UHMWPE	60–70	30–40

2.5. Wear Debris Extraction Rate

The wear debris extraction rate was used to quantify the extraction effect of wear debris under different extraction conditions. The wear debris extraction rate refers to the number of wear debris at the end of extraction as a percentage of the total wear debris before extraction and is calculated by the following formula.

$$RR = \frac{(m_1 - m_2)}{m} \times 100\% \quad (16)$$

m , m_1 , and m_2 are the mass of wear debris added before extraction, the total mass of filter paper and wear debris after centrifugal separation of wear debris for extraction, and the net mass of filter paper after removal of wear debris for drying, respectively.

2.6. Wear Debris Composition Analysis

To ensure that the mixed wear debris was completely separated from the rest of the calf serum and that no impurities were incorporated, compositional analysis of the post-extraction wear debris was performed. The consistency of the composition of the post-extraction wear debris with that of the wear debris added before the experiment was judged. Determination of the composition of CoCrMo wear debris after extraction from the lower zone of the CoCrMo/UHMWPE group by X-ray energy spectrometer (XflashFQ5060, Bruker, Shanghai, China). The composition of ZrO₂ particles in the ZrO₂/UHMWPE group was determined using X-ray energy spectrometry, and the abrasive chips were observed with a field emission transmission electron microscope (TEM) (SU8220, Hitachi, Ltd., Beijing, China). The composition of PEEK and other groups of UHMWPE particles in the PEEK/UHMWPE group was determined by infrared spectroscopy.

3. Results

3.1. Effect of Different Centrifugation Time and Isolation Times on Recovery Rate of Mixed Wear Debris in CoCrMo/UHMWPE Group

The fourth separation of CoCrMo and UHMWPE extracted too few pieces of wear debris, all of which could not be weighed. Therefore, the first three centrifugal separations

and extractions were taken into account. When the centrifugation time was 1 h, 2 h, 3 h, and 4 h, the first extraction rate of CoCrMo wear debris was 80.31%, 84.49%, 85.38%, and 85.46%, respectively. The extraction rate of wear debris increased by 4.18% more when centrifuged for two hours than when centrifuged for 1 h, and wear debris extraction rate increased by 0.89% and 0.97% more when centrifuged for 3 h and 4 h than when centrifuged for 2 h, respectively. The centrifugation was less than 2 h, and the extraction rate of CoCrMo wear debris was affected by the centrifugation time. The increase in extraction rate for CoCrMo wear debris was smaller as the centrifugation time increased. The first extraction rate of UHMWPE wear debris was 53.92%, 58.86%, 61.32%, and 63.20% when the centrifugation time was 1 h, 2 h, 3 h, and 4 h, respectively. The extraction rate of UHMWPE wear debris increased by 4.94% when the centrifugation time was 2 h compared with 1 h and increased by 2.46% and 4.34% when centrifugation was 3 h and 4 h compared with 2 h, respectively. When the centrifugation time was less than 2 h, the extraction rate of UHMWPE wear debris increased faster with the increase of centrifugation time. However, the extraction rate of UHMWPE wear debris did not increase significantly as the centrifugation time continued to rise. Centrifuged for 2 h, the second and third centrifugal separation extraction of CoCrMo wear debris increased the extraction rate by 3.9% and 6.34%, respectively, compared with the first centrifugal separation extraction. We reached a high level of extraction of CoCrMo wear debris by centrifugal separation. However, increases in centrifugal separation extraction resulted in wear debris extraction rates decreasing to below 4%. This indicates that even after increasing the number of centrifugal separations, growth in CoCrMo wear debris extraction rates was not evident. The extraction rates of UHMWPE wear debris were 58.86%, 16.79%, and 6.64%, respectively. With the increase of centrifugal separation extraction times, the extraction rate of UHMWPE wear debris gradually decreased, and the total extraction rate increased by 23.43% compared with the first extraction, so the extraction rate of UHMWPE wear debris could be significantly improved by increasing the number of centrifugal separation extraction times. The recovery rates of CoCrMo/UHMWPE mixed wear debris under different centrifugation methods are shown in Figure 5.

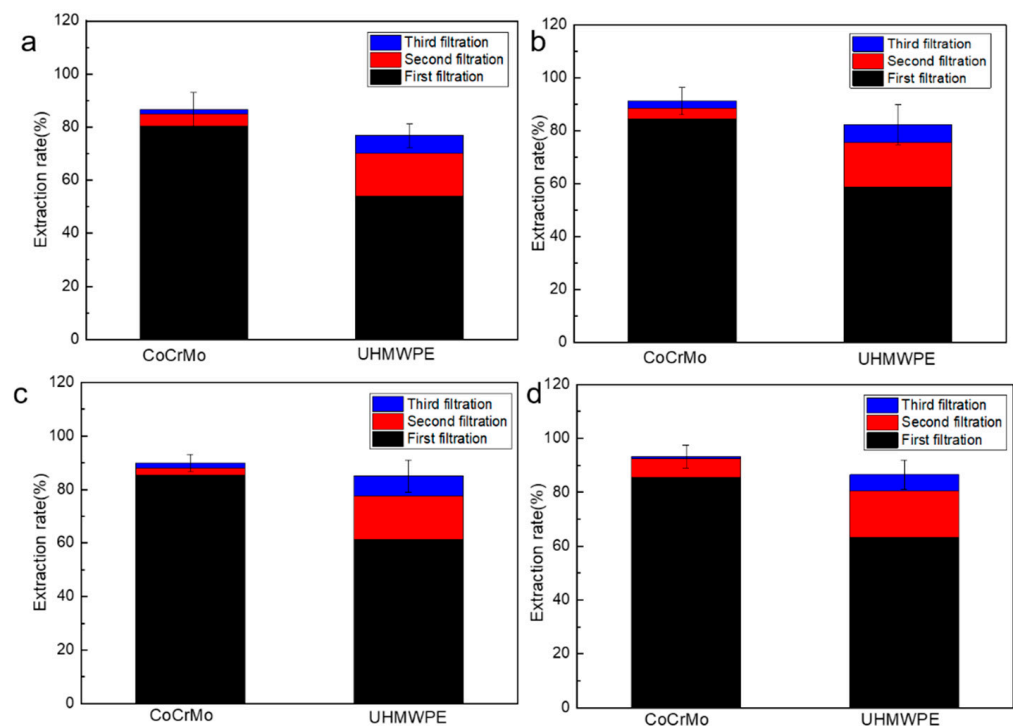


Figure 5. Recovery rate of CoCrMo/UHMWPE mixed particles with different centrifugation time and isolation times: (a) 1 h, (b) 2 h, (c) 3 h, and (d) 4 h.

3.2. Effect of Different Centrifugation Time and Isolation Times on Recovery Rate of Mixed Wear Debris in PEEK/UHMWPE Group

The fourth separation of PEEK and UHMWPE extracted too little wear debris, and both could not be weighed, so the results of the first three centrifugal separations and extraction were taken. The first extraction rates of PEEK wear debris were 77.21%, 82.00%, 82.95%, and 85.18% for centrifugation times of 1 h, 2 h, 3 h, and 4 h, respectively. The extraction rates of wear debris increased by 4.79%, 5.74%, and 7.97% for centrifugation times of 2 h, 3 h, and 4 h compared to 1 h, respectively. The extraction rate of PEEK wear debris was less influenced by the centrifugation time, and the first extraction rate grew slowly by continuing to increase the centrifugation time. The first extraction rates of UHMWPE wear debris were 38.58%, 73.71%, 75.59%, and 78.89% for centrifugation times of 1 h, 2 h, 3 h, and 4 h, respectively. The extraction rate of UHMWPE wear debris increased by 35.13% for centrifugation time of 2 h compared to centrifugation for 1 h. The extraction rate of UHMWPE wear debris increased by 1.88% and 5.18% compared to 2 h when the centrifugation time was 3 h and 4 h, respectively. Comparing the results of multiple centrifugation separations, the total extraction rate of PEEK wear debris reached 88.08%, and UHMWPE wear debris reached 85.13% after three extractions at a centrifugation time of 2 h. The extraction rates of PEEK and UHMWPE wear debris decreases as the number of centrifugal separations increases, and the single extraction rate of UHMWPE is a larger percentage of the total extraction rate than that of PEEK. In summary, increasing the number of centrifugal separations can increase the extraction rate of both PEEK and UHMWPE wear debris, and the total extraction rate of UHMWPE wear chips increased more significantly. The recoveries of PEEK/UHMWPE mixed wear debris at different centrifugation times are shown in Figure 6.

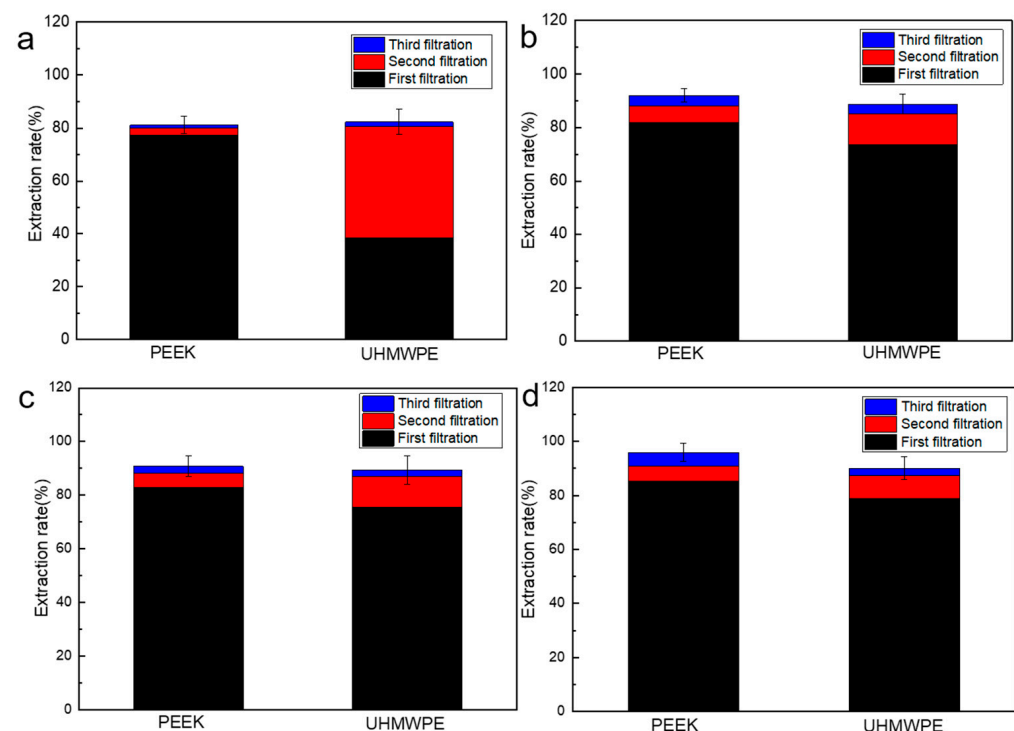


Figure 6. Recovery rate of PEEK/UHMWPE mixed particles with different centrifugation time and isolation times: (a) 1 h, (b) 2 h, (c) 3 h, and (d) 4 h.

3.3. Effect of Different Centrifugation Time and Isolation Times on Recovery Rate of Mixed Wear Debris in ZrO₂/UHMWPE Group

In the fourth separation of ZrO₂ and UHMWPE, so little wear debris were extracted that it was impossible to weigh them, so the results of the first three centrifugal separations and extractions were used. The extraction rates of ZrO₂ wear debris were 80.41%, 88.93%,

89.24%, and 90.20% for centrifugation times of 1 h, 2 h, 3 h, and 4 h, respectively. In a centrifugation time of 2 h, the extraction rate of ZrO_2 wear debris increased by 8.52% compared to 1 h. The extraction rate of ZrO_2 wear debris no longer increased significantly with the increase of centrifugation time when the centrifugation time was greater than 2 h. The extraction yield of UHMWPE wear debris was 61.59%, 72.01%, 72.50%, and 74.82% for centrifugation times of 1 h, 2 h, 3 h, and 4 h, respectively. Abstraction rate of UHMWPE wear debris increased by 10.42% for centrifugation time of 2 h compared with centrifugation of 1 h, and the extraction rate of wear debris increased by 0.49% and 2.81% for centrifugation of 3 h and 4 h compared with centrifugation of 2 h. Continued increase of centrifugal time has less effect on the extraction rate of UHMWPE wear debris. The extraction rate of both types of wear debris increased significantly with multiple centrifugations. As shown above, increasing the number of centrifugation extraction times can significantly improve the extraction rates of ZrO_2 and UHMWPE wear debris. The recoveries of ZrO_2 /UHMWPE mixed wear debris under different centrifugation methods are shown in Figure 7.

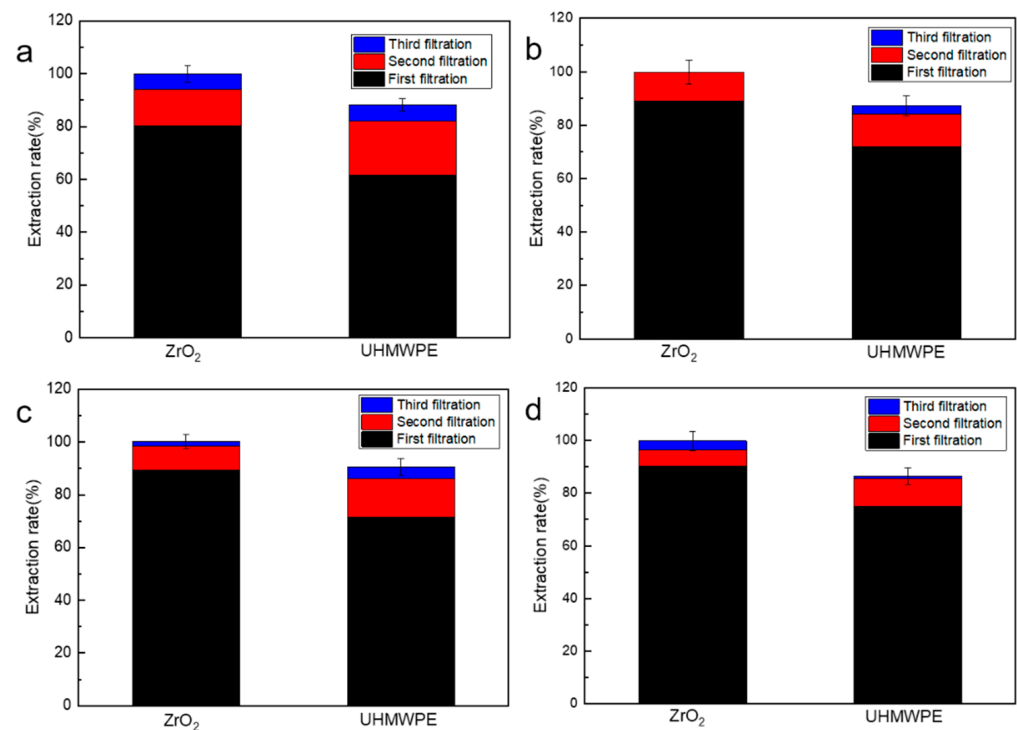


Figure 7. Recovery rate of ZrO_2 /UHMWPE mixed wear debris with different centrifugation time and isolation times: (a) 1 h, (b) 2 h, (c) 3 h, and (d) 4 h.

3.4. Component Identification of Wear Debris Isolated

3.4.1. Analysis of the Composition of CoCrMo/UHMWPE Mixed Wear Debris after Extraction

The results of energy spectrum analysis showed that Co, Cr, and Mo elements were only detected in the region containing CoCrMo wear debris. It could be determined that the extracted wear debris were CoCrMo, and no protein contamination or UHMWPE was found. The results are shown in Figure 8.

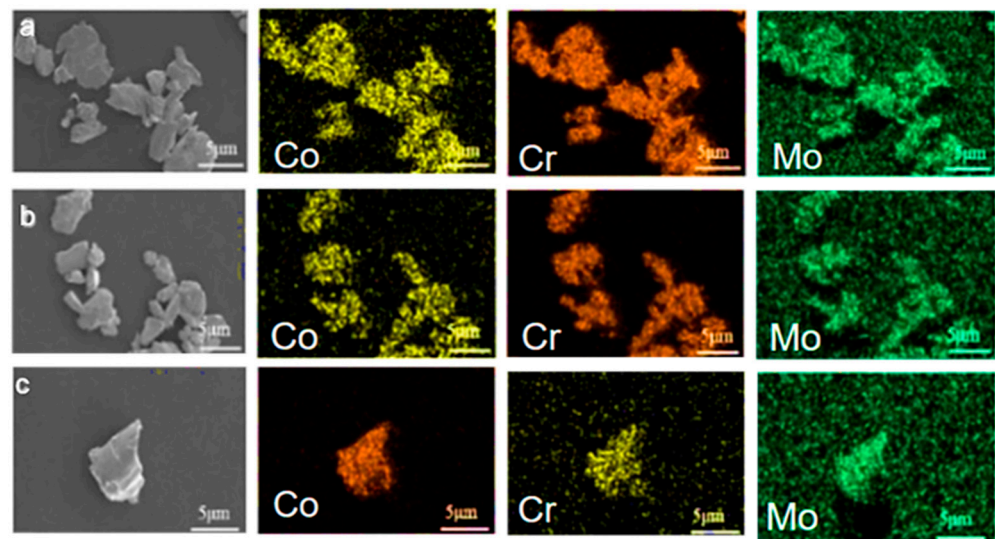


Figure 8. Elemental analysis of isolated CoCrMo wear debris: (a) first time, (b) second time, and (c) third time.

The FT-IR result (Figure 9) showed that the absorption curves of solution-extracted UHMWPE wear debris in the upper zone were consistent with those of UHMWPE wear debris before extraction. Absorption peaks were at 2919 cm^{-1} ($-\text{CH}_2-$, asymmetric stretching vibration), 2850 cm^{-1} ($-\text{CH}_2-$, symmetric stretching vibration), 1463 cm^{-1} ($-\text{CH}_2-$, bending vibration), and 719 cm^{-1} ($-(\text{CH}_2)_n-$, $n \geq 4$ in-plane rocking vibration).

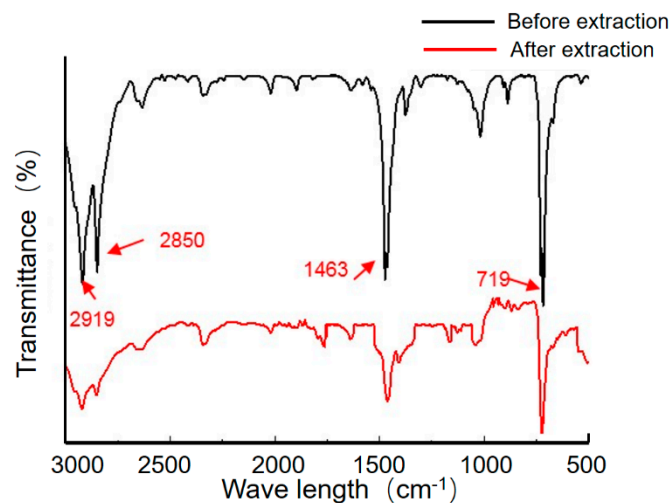


Figure 9. FTIR spectra of isolated wear debris in upper zone of CoCrMo/UHMWPE group and non-isolated UHMWPE wear debris.

3.4.2. Post-Extraction Composition Analysis of Mixed Wear Debris of PEEK/UHMWPE Group

The FT-IR result (Figure 10) shown that the infrared absorption curves of PEEK wear debris after extraction and before extraction were consistent. Absorption peaks at 1652 cm^{-1} ($\text{C}=\text{O}$ stretching vibration), 1501 cm^{-1} , 1579 cm^{-1} (in-plane vibration of benzene ring), 1226 cm^{-1} ($\text{R}-\text{O}-\text{R}$ asymmetric stretching vibration), 1163 cm^{-1} (in-plane $\text{C}-\text{H}$ bending vibration of aromatic ether or aromatic ketone benzene ring), 840 cm^{-1} , 764 cm^{-1} (out-of-plane $\text{C}-\text{H}$ bending vibration of benzene ring). bending vibration), 840 cm^{-1} , and 764 cm^{-1} ($\text{C}-\text{H}$ out-of-plane bending vibration of benzene ring) appeared, which could indicate that the composition of the wear debris before and after extraction was PEEK. There was no admixture of UHMWPE wear debris or protein particles. The FT-IR result (Figure 11)

showed the infrared spectral absorption curves of UHMWPE wear debris obtained from the upper zone solution extraction were the same as before extraction. The positions of the absorption peaks of the UHMWPE wear debris extracted from the upper zone solution and before extraction are the same, indicating that the wear debris extracted from the upper zone solution are UHMWPE. The PEEK wear debris and protein wear debris as well as other impurities are not mixed in the extraction process.

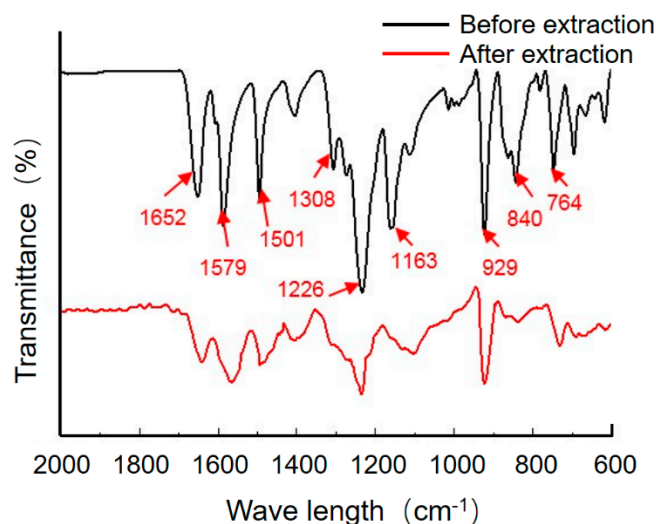


Figure 10. FTIR spectrum of isolated wear debris in lower zone of PEEK/UHMWPE group and non-isolated PEEK wear debris.

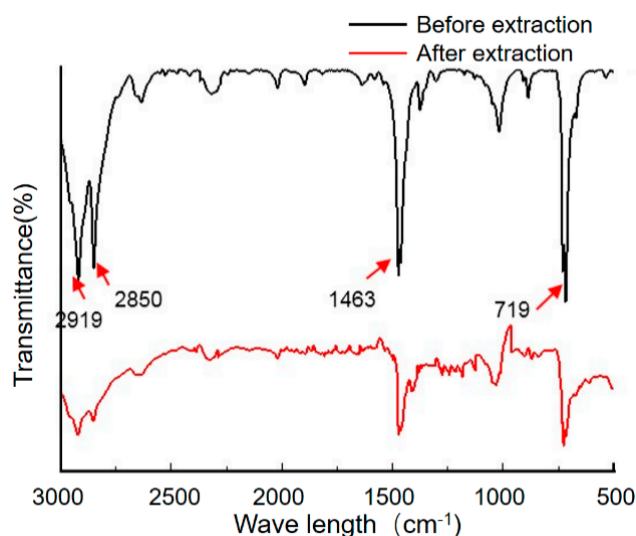


Figure 11. FTIR spectrum of isolated wear debris in upper zone of PEEK/UHMWPE group and non-isolated UHMWPE wear debris.

3.4.3. Analysis of Wear Debris Composition after Extraction in ZrO₂/UHMWPE Group

EDS analysis (Figure 12) of solution-extracted wear debris from the lower zone of ZrO₂/UHMWPE showed that ZrO₂ wear debris agglomerated and formed large particle clusters. Zr and O elements occur around particle clusters and also sporadically in the area outside the particle clusters. It can be determined that the extracted wear debris are ZrO₂ wear debris and occur as large particle clusters, small particle clusters, or individual particles. FT-IR (Figure 13) showed that the material structure of the extracted wear debris in the upper zone solution was the same as before extraction, indicating that the extracted wear debris in the upper zone were UHMWPE. The extracted wear debris were not mixed with ZrO₂ or other impurities.

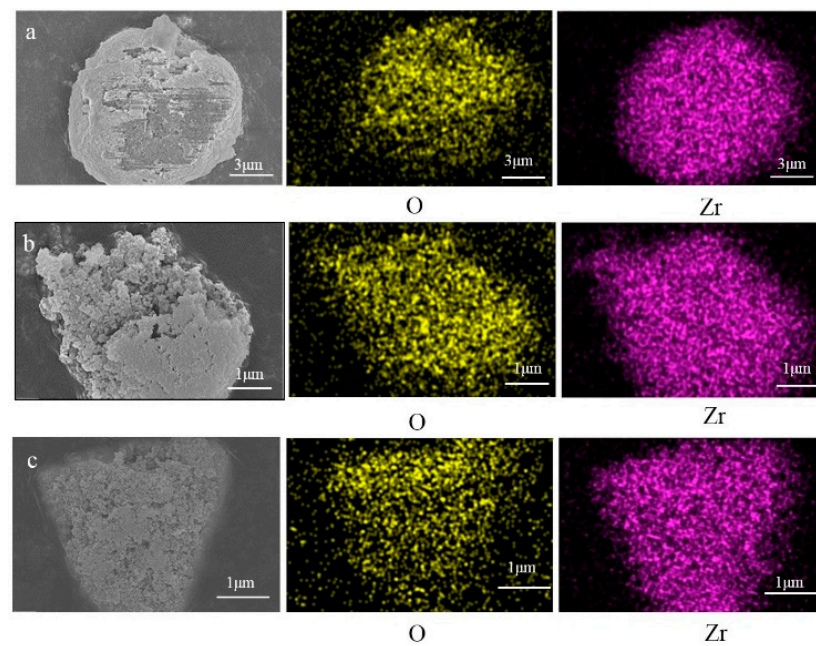


Figure 12. Elemental analysis of isolated ZrO_2 wear debris; (a) isolated ZrO_2 wear debris after first centrifugation; (b) isolated ZrO_2 wear debris after second centrifugation; (c) isolated ZrO_2 wear debris after third centrifugation.

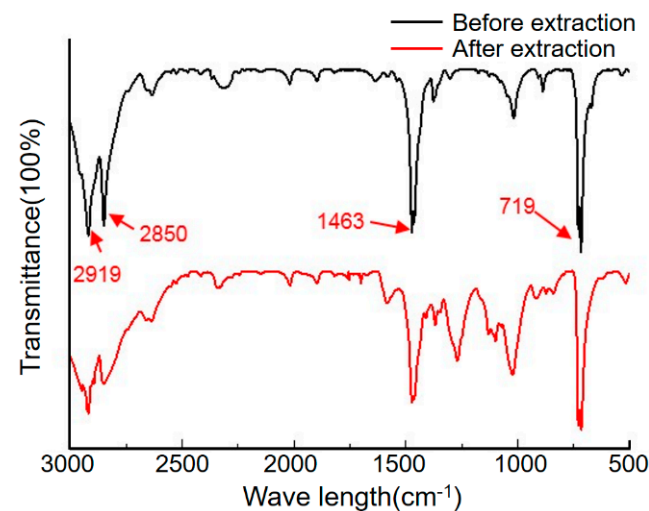


Figure 13. FTIR spectrum of isolated wear debris in upper zone of PEEK/UHMWPE group and non-isolated UHMWPE wear debris.

4. Discussion

In the natural state, the particle settling velocity is closely related to the particle density, radius, shape, and solvent viscosity, where the density and radius have a substantial impact [36]. In this study, high-speed centrifugation at 10,000 r/min was used to accelerate the floating or sinking of different densities of wear debris. To achieve complete separation of two different densities of artificially jointed mixed wear debris. Under centrifugal settling conditions, the disturbance flow around the wear debris is dominated by laminar and transitional types. The particles in solution are dispersed by van der Waals forces, electrostatic repulsion, capillary forces, and other interactions of particles combined with each other into clusters of particles of different diameters and dispersion. As shown by the Stokes formula, the particle stabilization phase settling velocity is proportional to the square of the particle diameter, and particle clusters rather than a single particle settling velocity increases significantly. This type of settlement is called “group sedimentation”

(Figure 14a). Group sedimentation can accelerate particle sedimentation and facilitate the separation and extraction of particles of different densities in solution.

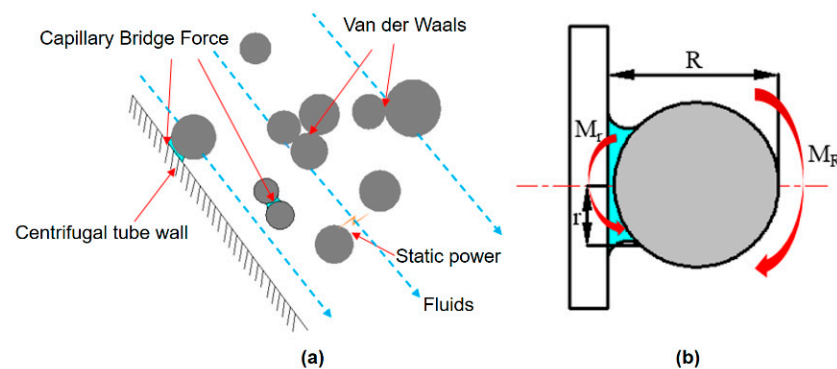


Figure 14. (a) Schematic diagram of fine particle flow in centrifugal tube; (b) schematic diagram of removal mechanism of particles attached to centrifugal tube wall.

Under the wetting condition of the centrifuge tube wall, capillary forces were formed between the micro-particles and the centrifuge tube wall. The capillary forces are mainly due to the irregular surface morphology of the micro-particles. The presence of many micro-spaces or micro-gaps between the micro-particles or micro-particle clusters and the centrifuge tube surface. The capillary liquid bridge force between the particle hydrate and the centrifuge tube wall is the main adhesion force; the force is proportional to the particle radius (Figure 14b). The removal moment applied to the hydrate particles is less than the capillary liquid bridge force, and the hydrate particles adhere to the tube wall. When the removal forces on the hydrate particles were greater than the capillary bridge force, the particles leave the tube wall [37–39]. When the external force on the particle is greater than the static friction of the particle, the removal moment M_R of the hydrate particle is greater than the impedance moment M_r , and the particle can be removed by rolling. The surface of the centrifuge tubes wall is rinsed with deionized water, in which the force of the water flow is greater than the force of the micro-particles adhering to the tube wall, and the micro-particles roll with the water flow on the surface of the centrifuge tube and finally leave the surface of the tube with the water flow. Therefore, extraction by multiple centrifugation can rinse the particles attached to the wall of the centrifuge tube after the last filtration into the solution for another centrifugation, which in turn collects more particles and achieves a higher extraction rate. The extraction rate growth of PEEK and UHMWPE wear debris was significantly higher than that of CoCrMo and ZrO_2 ceramic wear debris using multiple centrifugal extraction separation extraction methods.

5. Conclusions

In this study, an extraction method of multiple centrifugal separations of different density ratios of artificial joint mixed wear debris were proposed, and the optimal centrifugal time and number of centrifugal separations were determined.

By increasing the centrifugation time to improve the extraction rate of wear debris, the increase in extraction rate of wear debris by centrifugation for 2 h versus centrifugation for 1 h is as follows: The extraction rate of CoCrMo and UHMWPE wear debris respectively increased by 47.19% and 4.94% in the CoCrMo/UHMWPE group. The extraction rate of PEEK and UHMWPE wear debris increased by 4.76% and 35.13% in PEEK/UHMWPE group. The extraction rate of ZrO_2 wear debris increased by 8.52%, and UHMWPE increased by 10.42% in ZrO_2 /UHMWPE group. It was first proposed to increase the extraction rate of grinding chips by increasing the number of centrifugal separation extractions. After four centrifugal extractions with a centrifugal time of 2 h, the extraction rates of CoCrMo and UHMWPE wear debris in the CoCrMo/UHMWPE group reached 84.49% and 82.29%. The total extraction rates increased by 6.7% and 23.44%, respectively, compared with single centrifugal extraction. The extraction rates of PEEK and UHMWPE wear debris in

the PEEK/UHMWPE group increased by 9.95% and 15.1%, respectively, compared with single centrifugal extraction. The extraction rates of ZrO₂ and UHMWPE wear debris in ZrO₂/UHMWPE group increased by 10.91% and 15.32%, respectively, compared with single centrifugal extraction. The multiple centrifugal separation and extraction effectively collected the abrasive debris from the wall of the centrifuge tube, and the abrasive debris extraction rate reached a relatively high level.

The research results of this paper are of great significance to the analysis of artificial knee joint materials and artificial knee joint wear characteristics, generation mechanism, and wear mechanism. It has important reference value for the prediction of the artificial knee joint life and prolongation of the artificial knee joint life and provides theoretical reference for the development and promotion of new artificial joints.

Author Contributions: Conceptualization, C.F. and T.Z.; methodology, Y.Z.; software, T.Z.; validation, C.F., Y.Z.; formal analysis, C.F. and Y.Z.; investigation, C.F., and Y.Z.; resources, T.Z.; data curation, C.F., Y.Z.; writing—original draft preparation, Y.Z.; writing—review and editing, C.F.; visualization, C.F. and Y.Z.; supervision, D.Z.; project administration, K.C., X.L. and D.Z. All authors have read and agreed to the published version of the manuscript.

Funding: This study was supported by the National Natural Science Foundation of China (No. 51875564, 52105231 and 52175204), Natural Science Foundation of Jiangsu Province (Grant No. BK20211243), the Fundamental Research Funds for the Central Universities (2021QN1108), the Tribology Science Fund of State Key Laboratory of Tribology (Grant No. SKLTKF21B15), and the Open Fund of State Key Laboratory of Solid Lubrication, Lanzhou Institute of Chemical Physics (Grant No. LSL-2107).

Data Availability Statement: Not applicable.

Conflicts of Interest: The authors who have taken part in this study declared that they do not have anything to disclose regarding funding or conflict of interest with respect to this manuscript.

References

1. Yoneyama, C.; Cao, S.; Munoz, A.I.; Mischler, S. Influence of Bovine Serum Albumin (BSA) on the Tribocorrosion Behaviour of a Low Carbon CoCrMo Alloy in Simulated Body Fluids. *Lubricants* **2020**, *8*, 61. [[CrossRef](#)]
2. DeLee, J.G.; Charnley, J. Radiological demarcation of cemented sockets in total hip replacement. *Clin. Orthop. Relat. Res.* **1976**, *121*, 20–32. [[CrossRef](#)]
3. Chiesa, R.; Tanzi, M.; Alfonsi, S.; Paracchini, L.; Moscatelli, M.; Cigada, A. Enhanced wear performance of highly crosslinked UHMWPE for artificial joints. *J. Biomed. Mater. Res.* **2000**, *50*, 381–387. [[CrossRef](#)]
4. Kyomoto, M.; Moro, T.; Takatori, Y.; Tanaka, S.; Ishihara, K. Multidirectional Wear and Impact-to-wear Tests of Phospholipid-polymer-grafted and Vitamin E-blended Crosslinked Polyethylene: A Pilot Study. *Clin. Orthop. Relat. Res.* **2015**, *473*, 942–951. [[CrossRef](#)] [[PubMed](#)]
5. Moro, T.; Takatori, Y.; Kyomoto, M.; Ishihara, K.; Kawaguchi, H.; Hashimoto, M.; Tanaka, T.; Oshima, H.; Tanaka, S. Wear resistance of the biocompatible phospholipid polymer-grafted highly cross-linked polyethylene liner against larger femoral head. *J. Orthop. Res.* **2015**, *33*, 1103–1110. [[CrossRef](#)]
6. Hongtao, L.; Shirong, G.; Shoufan, C.; Shibo, W. Comparison of wear debris generated from ultra high molecular weight polyethylene in vivo and in artificial joint simulator. *Wear* **2011**, *271*, 647–652. [[CrossRef](#)]
7. Minoda, Y.; Kobayashi, A.; Iwaki, H.; Miyaguchi, M.; Kadoya, Y.; Ohashi, H.; Takaoka, K. Characteristics of polyethylene wear particles isolated from synovial fluid after mobile-bearing and posterior-stabilized total knee arthroplasties. *J. Biomed. Mater. Res. B* **2004**, *71*, 1–6. [[CrossRef](#)]
8. McMullin, B.; Leung, M.; Shanbhag, A.; McNulty, D.; Mabrey, J.; Agrawal, C. Correlating subjective and objective descriptors of ultra high molecular weight wear particles from total joint prostheses. *Biomaterials* **2006**, *27*, 752–757. [[CrossRef](#)]
9. Matthews, J.B.; Besong, A.A.; Green, T.R.; Stone, M.H.; Wroblewski, B.M.; Fisher, J.; Ingham, E. Evaluation of the response of primary human peripheral blood mononuclear phagocytes to challenge with In vitro generated clinically relevant UHMWPE particles of known size and dose. *J. Biomed. Mater. Res.* **2000**, *52*, 296–307. [[CrossRef](#)]
10. Halim, T.; Clarke, I.C.; Burgett-Moreno, M.D.; Donaldson, T.K.; Savisaar, C.; Bowsher, J.G. A simulator study of adverse wear with metal and cement debris contamination in metal-on-metal hip bearings. *Bone Jt. Res.* **2015**, *4*, 29–37. [[CrossRef](#)]
11. Halim, T.; Burgett, M.; Donaldson, T.K.; Savisaar, C.; Bowsher, J.; Clarke, I.C. Profiling the third-body wear damage produced in CoCr surfaces by bone cement, CoCr, and Ti6Al4V debris: A 10-cycle metal-on-metal simulator test. *Proc. Inst. Mech. Eng. Part H* **2014**, *228*, 703–713. [[CrossRef](#)] [[PubMed](#)]

12. Brown, C.; Williams, S.; Tipper, J.L.; Fisher, J.; Ingham, E. Characterisation of wear particles produced by metal on metal and ceramic on metal hip prostheses under standard and microseparation simulation. *J. Mater. Sci. Mater. Med.* **2007**, *18*, 819–827. [[CrossRef](#)] [[PubMed](#)]
13. Milosev, I.; Remskar, M. In vivo production of nanosized metal wear debris formed by tribochemical reaction as confirmed by high-resolution TEM and XPS analyses. *J. Biomed. Mater. Res. Part A* **2009**, *91*, 1100–1110. [[CrossRef](#)] [[PubMed](#)]
14. McKee, G.K.; Watson-Farrar, J. Replacement of arthritic hips by the McKee-Farrar prosthesis. *J. Bone Jt. Surg.* **1966**, *48*, 245–259. [[CrossRef](#)]
15. Tuan, R.S.; Lee, F.Y.; Konttinen, Y.T.; Wilkinson, J.M.; Smith, R.L. What are the local and systemic biologic reactions and mediators to wear debris, and what host factors determine or modulate the biologic response to wear particles? *J. Am. Acad. Orthop. Surg.* **2008**, *16*, S42–S48. [[CrossRef](#)]
16. Ingham, E.; Fisher, J. The role of macrophages in osteolysis of total joint replacement. *Biomaterials* **2005**, *26*, 1271–1286. [[CrossRef](#)]
17. Bitar, D.; Parvizi, J. Biological response to prosthetic debris. *World, J. Orthop.* **2015**, *6*, 172–189. [[CrossRef](#)]
18. Huang, C.; Lu, Y.; Chang, T.; Hsiao, I.; Su, Y.; Yeh, S.; Fang, H.; Huang, C. In vivo biological response to highly cross-linked and vitamin e-doped polyethylene particle-Induced osteolysis animal study. *J. Biomed. Mater. Res. Part B* **2016**, *104*, 561–567. [[CrossRef](#)]
19. Ingham, E.; Fisher, J. Biological reactions to wear debris in total joint replacement. *Proc. Inst. Mech. Eng. Part H* **2000**, *214*, 21–37. [[CrossRef](#)]
20. Affatato, S.; Bersaglia, G.; Rocchi, M.; Taddei, P.; Fagnano, C.; Toni, A. Wear behaviour of cross-linked polyethylene assessed in vitro under severe conditions. *Biomaterials* **2005**, *26*, 3259–3267. [[CrossRef](#)]
21. Smith, A.M.; Fleming, L.; Wudebwe, U.; Bowen, J.; Grover, L.M. Development of a synovial fluid analogue with bio-relevant rheology for wear testing of orthopaedic implants. *J. Mech. Behav. Biomed. Mater.* **2014**, *32*, 177–184. [[CrossRef](#)] [[PubMed](#)]
22. Ghosh, S.; Choudhury, D.; Roy, T.; Moradi, A.; Masjuki, H.H.; Pingguan-Murphy, B. Tribological performance of the biological components of synovial fluid in artificial joint implants. *Sci. Technol. Adv. Mater.* **2015**, *16*, 045002. [[CrossRef](#)] [[PubMed](#)]
23. Visentin, M.; Stea, S.; Squarzone, S.; Antonietti, B.; Reggiani, M.; Toni, A. A new method for isolation of polyethylene wear debris from tissue and synovial fluid. *Biomaterials* **2004**, *25*, 5531–5537. [[CrossRef](#)]
24. Singh, J.; Sloan, J.A.; Johanson, N.A. Challenges with Health-related Quality of Life Assessment in Arthroplasty Patients: Problems and Solutions. *J. Am. Acad. Orthop. Surg.* **2010**, *18*, 72–82. [[CrossRef](#)]
25. Kurtz, S.M.; Austin, M.S.; Azzam, K.; Sharkey, P.F.; MacDonald, D.W.; Medel, F.J.; Hozack, W.J. Mechanical Properties, Oxidation, and Clinical Performance of Retrieved Highly Cross-Linked Crossfire Liners After Intermediate-Term Implantation. *J. Arthroplast.* **2010**, *25*, 614–623. [[CrossRef](#)]
26. Park, D.Y.; Min, B.H.; Kim, D.W.; Song, B.R.; Kim, M.; Kim, Y.J. Polyethylene wear particles play a role in development of osteoarthritis via detrimental effects on cartilage, meniscus, and synovium. *Osteoarthr. Cartil.* **2013**, *21*, 2021–2029. [[CrossRef](#)] [[PubMed](#)]
27. Pourzal, R.; Catelas, I.; Theissmann, R.; Kaddick, C.; Fischer, A. Characterization of wear particles generated from CoCrMo alloy under sliding wear conditions. *Wear* **2011**, *271*, 1658–1666. [[CrossRef](#)]
28. Gajski, G.; Jelcic, Z.; Orescanin, V.; Geric, M.; Kollar, R.; Garaj-Vrhovac, V. Physico-chemical characterization and the in vitro genotoxicity of medical implants metal alloy (TiAlV and CoCrMo) and polyethylene particles in human lymphocytes. *BBA-Gen. Subj.* **2014**, *1840*, 565–576. [[CrossRef](#)]
29. Anand, L. Plane deformations of ideal granular materials[†]. *J. Mech. Phys. Solids* **1983**, *31*, 105–122. [[CrossRef](#)]
30. Cheng, N. Comparison of formulas for drag coefficient and settling velocity of spherical particles. *Powder Technol.* **2009**, *189*, 395–398. [[CrossRef](#)]
31. Markauskas, D.; Kruggel-Emden, H.; Sivanesapillai, R.; Steeb, H. Comparative study on mesh-based and mesh-less coupled CFD-DEM methods to model particle-laden flow. *Powder Technol.* **2017**, *305*, 78–88. [[CrossRef](#)]
32. Fan, L. Multiphase flow and fluidization: Continuum and kinetic theory descriptions. *AIChE J.* **1996**, *42*, 1197–1198. [[CrossRef](#)]
33. Jenny, M.; Souhar, M. Numerical simulation of a film coating flow at low capillary numbers. *Comput. Fluids* **2009**, *38*, 1823–1832. [[CrossRef](#)]
34. Leung, W. Separation of dispersed suspension in rotating test tube. *Sep. Purif. Technol.* **2004**, *38*, 99–119. [[CrossRef](#)]
35. Richardson, J.F.; Zaki, W.N. The sedimentation of a suspension of uniform spheres under conditions of viscous flow. *Chem. Eng. Sci.* **1954**, *3*, 65–73. [[CrossRef](#)]
36. Larsen, T. Measuring the variations of the apparent settling velocity for fine particles. *Water Res.* **2000**, *34*, 1417–1418. [[CrossRef](#)]
37. Sanchez-Reyes, J.; Archer, L. Interfacial slip violations in polymer solutions: Role of microscale surface roughness. *Langmuir* **2003**, *19*, 3304–3312. [[CrossRef](#)]
38. Wang, S.; Drda, P.A. Superfluid-Like Stick–Slip Transition in Capillary Flow of Linear Polyethylene Melts. 1. General Features. *Macromolecules* **1996**, *29*, 2627–2632. [[CrossRef](#)]
39. Brochard, F.; De Gennes, P.G. Shear-dependent slippage at a polymer/solid interface. *Langmuir* **1992**, *8*, 3033–3037. [[CrossRef](#)]